# Real-Time Digital Simulation of Microgrid Control Strategies

Chanaka Keerthisinghe*, *Member, IEEE,* Daniel S. Kirschen*, *Fellow, IEEE*, and Scott Gibson†

*Department of Electrical and Computer Engineering, University of Washington, Seattle, Washington 98195, USA

†Snohomish County Public Utility District, Everett, Washington 98201, USA

Email: chanakak@uw.edu, kirschen@uw.edu and hsgibson@snopud.com

*Abstract*—This paper evaluates microgrid control strategies prior to actual implementation using a real-time digital simulator. The microgrid model includes photovoltaic generation, a battery, an emergency generator, loads and a vehicle-to-grid enabled electric vehicle charging station. Three operational scenarios are studied: grid-connected operation; seamless transition to islanded mode with the battery inverter operating in grid-forming mode; and islanded operation using the emergency generator when the battery is discharged.

*Index Terms*—microgrid, real-time digital simulation, OPAL-RT®, Simulink®

## I. Introduction

REAL-TIME digital simulations can be used to evaluate and design microgrid control strategies without any risk prior to actual deployment in the field [1]–[8].

This paper describes a model of the microgrid that the Snohomish County Public Utility District (Snohomish PUD) is building in Arlington, Washington State. This microgrid is currently in the design stage and is expected to be completed by the end of 2020 [9]. It consists of PV generation, a battery, an emergency generator, loads and a vehicle-to-grid (V2G) enabled electric vehicle (EV) charging station. When the microgrid is synchronized to the main grid, the battery will be used for solar smoothing, peak-shaving and energy arbitrage. The battery and PV inverters will then operate in grid-following mode. On the other hand, when the microgrid is islanded, the battery inverter will operate in grid-forming mode while the PV inverter will operate in grid-following mode. The emergency generator will only be used when the battery is discharged and there is insufficient PV generation. The batteries of the EVs are capable of supporting the microgrid and the electrical grid. The simulation models developed in MathWorks® Simulink® using the Simscape Power Systems™ (formerly SimPowerSystems™) toolbox are available to the public and could be adapted to model other microgrids [10].

The rest of the paper is structured as follows: Section II presents the Simulink® models of the microgrid. Section III describes the setup used for the real-time digital simulation. Section IV presents simulation results for different operating scenarios. Section V draws conclusions and outlines future work.
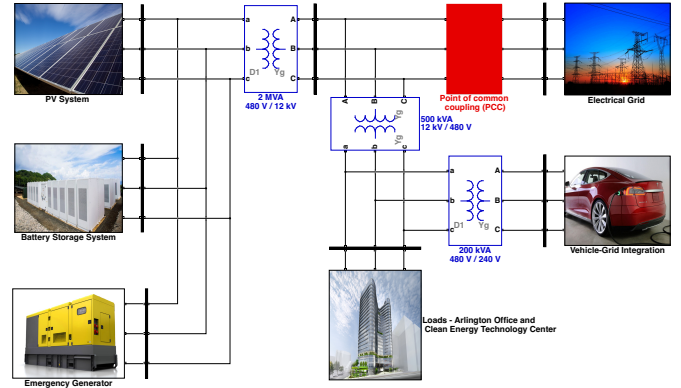


Fig. 1. Components of the Arlington Microgrid.

TABLE I
SPECIFICATIONS OF THE REC TWINPEAK 2S MONO 72 SERIES 375 W PV MODULE

| Parameters | Values |
|---|---|
| Maximum power | 375 W |
| Open circuit voltage (Voc) | 48 V |
| Rated Voltage (Vr) | 40.1 V |
| Short circuit current (Isc) | 9.96 A |
| Rated current (Ir) | 9.36 A |
| Temperature coefficient of Voc | -0.28 %/C |
| Temperature coefficient of Isc | 0.04 %/C |
| Number of cells per module | 144 |

## II. Microgrid Model

Figure 1 shows the connections between the various components of the microgrid. The following subsections describe in detail how each of these components is modeled.

### A. PV System

The PV system consists of the PV array, maximum power point tracker (MPPT) and an inverter. The PV array [11] consists of multiple PV modules connected in series and parallel to achieve the desired voltage and current. Table I provides the specifications of the PV modules. The PV array consists of 1640 modules divided into four sub-arrays, each of which contains 410 modules organized in 41 strings of 10 series-connected modules, and is rated at 615 kWdc.

Fig. 2 shows the current-voltage and power-voltage characteristics of each sub-array for different solar irradiances and temperatures. Each array is equipped with an MPPT to keep
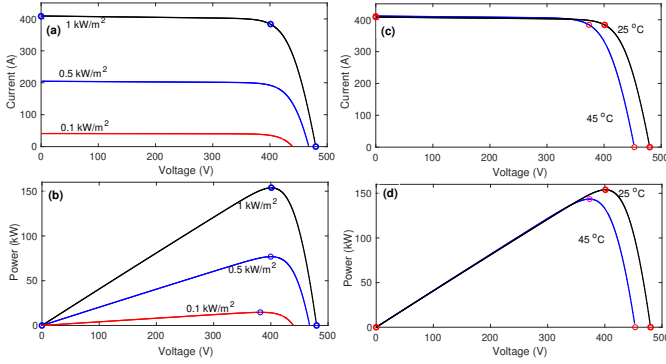
Fig. 2. PV sub-array current-voltage and power-voltage characteristics for different solar irradiances (a, b) and temperatures (c, d). The temperature value for diagrams a and b is $25\,^{0}$C while the solar irradiance for diagrams c and d is 1000 W/m$^{2}$.

the voltage at the the maximum power point (MPP) as the solar irradiance and the temperature of the panel change. This tracking is achieved using a DC-DC converter that implements a *perturb and observe* algorithm. Note that the voltages on the PV array and the dc link can therefore be different. Another option would be to connect the PV array directly to the dc link of the inverter and to incorporate the MPPT algorithm in the controller of this inverter [12].

The PV inverter is a two-level three-bridge voltage source converter (VSC) that operates in grid-following mode. Fig. 3 summarizes the inverter control algorithm. The reference voltage and current signals for phase-locked-loop (PLL) are measured from the inverter output. The PLL and measurements block calculate the angle synchronized on the rising zero-crossing of the fundamental of the reference signal, and transform both voltages and currents from the abc to the dq0 reference frames.

When the input power from the solar array changes due to variation in irradiance or temperature, the DC link voltage also changes because the power obtained from the array does not match the power delivered to the grid. The function of the voltage regulator is thus to change the active power reference current ($I_d$) of the current regulator so that power obtained from the solar array matches the power delivered to the grid [13].

The current regulator uses the current references $I_d$ and $I_q$ (reactive current) to calculate the required reference voltages for the inverter. The reactive current reference is taken as 0 in this model, as the system only supplies active power to the grid. More details about this controller can be found in [14]. In this model, the harmonics produced by the inverter are filtered using a single inductor (L). However, other filtering options are possible [13].

### B. Battery Energy Storage

The battery energy storage system consists of a Li-ion battery, a dc-dc converter and an inverter with both grid-forming and grid-following capabilities. Table II provides the specifications for the battery model [15]. A bi-directional DC-DC converter is inserted between the inverter and the battery to control the battery charge and discharge rates in grid-following
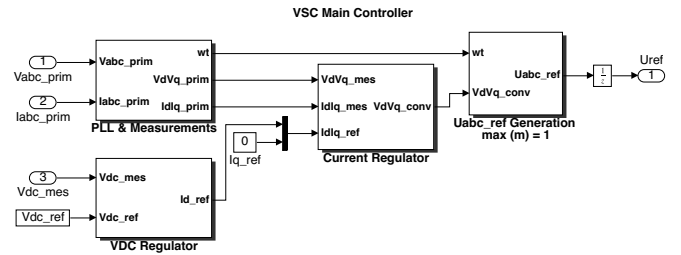


Fig. 3. Control of the PV inverter for grid-following operation.

TABLE II
SPECIFICATIONS OF THE BATTERY

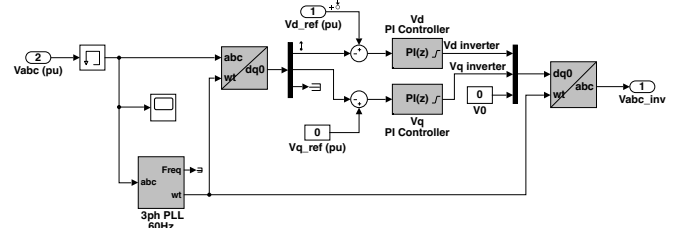| Parameters | Values |
|---|---|
| Nominal voltage | 800 V |
| Rated capacity | 1250 Ah |
| Fully charged voltage | 931.2 V |
| Maximum capacity | 1320 Ah |
| Capacity @nominal voltage | 1250 Ah |
| Nominal discharge current | 1250 A |
| Exponential zone voltage | 860 V |
| Exponential zone capacity | 60 Ah |
| Internal resistance | 0.0064 |



Fig. 4. Battery inverter operation as a voltage regulator during islanded operation.

mode [16]. The battery inverter control for grid-connected mode, which is similar to the PV inverter controller [12]. In islanded mode, this inverter controller operates as a voltage regulator as shown in Fig. 4.

### C. Emergency Generator

The emergency diesel generator consists of a synchronous generator, diesel engine governor and an excitation system, as shown in Fig. 5. The model of the synchronous machine takes into account the dynamics of the stator, field, and damper windings and is represented using a sixth-order model [17]. Table III. provides the specifications of this emergency generator.

In order to synchronise the emergency generator it's frequency, voltage magnitude and phase angle must be matched with those of the microgrid. The frequency of the emergency generator, $f_{\mathrm{g}}$ is given by:

$$n_s = \frac{120 f_{\mathrm{g}}}{P} \qquad (1)$$

where $n_s$ is the synchronous speed of the generator in revolutions per minute and $P$ is the number of poles. The desired frequency is obtained by changing the speed reference of the
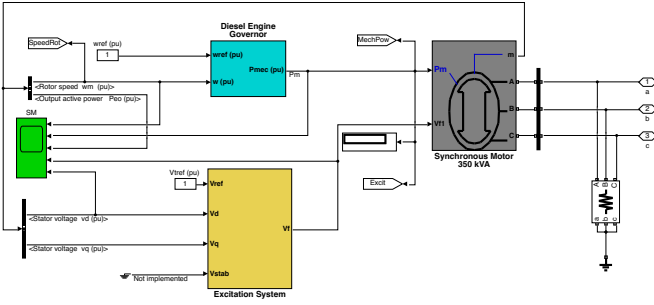
Fig. 5. Emergency generator model including synchronous machine, excitation system and diesel engine governor.

TABLE III
SPECIFICATIONS OF THE EMERGENCY GENERATOR

| Parameters | Values |
|---|---|
| Power rating | 350 kW |
| Voltage rating | 480 V |
| Frequency | 60 Hz |
| Stator resistance | 0.0036 $\Omega$ |
| Inertia coefficient | 20 |
| Pole pairs | 4 |



Fig. 6. Setup for power hardware-in-the-loop and software-in-the loop testing.

diesel engine governor, such that 1 pu corresponds to $f_g$=60 Hz, $P$=4, $n_s$=1800 rpm [18].

The generator voltage is adjusted by controlling the reference voltage of the excitation system. Note that a reference of 1 V (pu) corresponds to the rated voltage of the generator. The emergency generator is connected to the microgrid when the phase angle difference is close to zero [18].

### D. Vehicle-grid integration

The vehicle-grid integration system is modeled using an EV battery and an inverter that controls the charge and discharge rates. The EV battery has the specifications given in Table IV. An average model has been used for the DC-AC inverter, which is based on the work described in [19]–[21].

## III. REAL-TIME SIMULATION

Simulating this microgrid at 50 $\mu$s fixed time-steps in Simulink® over a long period of time requires an excessive amount of computing time. We also wanted to have the ability to perform hardware-in-the-loop simulations to test some of the components and their controllers. The Simulink® model

TABLE IV
SPECIFICATIONS OF THE EV BATTERY

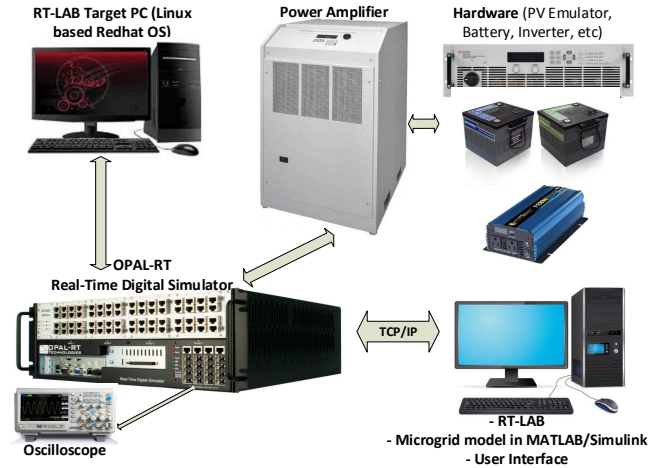| Parameters | Values |
|---|---|
| Nominal voltage | 200 V |
| Rated capacity | 500 Ah |
| Fully charged voltage | 232.8 V |
| Maximum capacity | 500 Ah |
| Capacity @nominal voltage | 452.2 Ah |
| Nominal discharge current | 217.4 A |
| Exponential zone voltage | 216.1 V |
| Exponential zone capacity | 24.6 Ah |
| Internal resistance | 0.004 |

was therefore ported to an OPAL-RT ® eMEGAsim real-time digital simulator [22]. The simulator hardware consists of an OP5600 chassis equipped with up to 12 parallel 3.3-GHz processor cores, a flexible high-speed front-end processor and a signal conditioning stage. The solver used is called ARTEMiS (advanced real-time electromagnetic simulation). Fig. 6 illustrates this real-time digital simulation testbed.

The Simulink® model of the microgrid is first to run as an effective platform for developing and testing the real-time microgrid. The Simulink® microgrid model has to be separated into different subsystems (master, slave, and console) in order to execute the model on several cores, before being compiled using RT-LAB. Each master and slave subsystem in RT-LAB is assigned to a separate core to perform their parallel processes in a fast and efficient way.

Power system models are typically decoupled at large transmission lines because these lines introduce a delay in signal propagation. Because there are obviously no such lines in a microgrid, we decoupled the system at dc busses. Another option is to use OPAL-RT's ARTEMiS state-space nodal (SSN) solver, which results in the same solution.

## IV. SIMULATION RESULTS AND DISCUSSION

This section discusses the simulation of three operating scenarios.

### A. Scenario A: Grid-connected operation

The microgrid is operated in grid-connected mode, with the PV system injecting a variable amount of power into the grid as solar irradiance changes. From t = 1 second to t = 60 seconds, the battery is used for solar smoothing. From t = 60 second to t = 100 seconds, the battery charges and discharges at a constant rate. From t = 50 second to t = 90 seconds, the active load varies. The EV is discharged at 50 kW from t = 0 second to t = 40 seconds and charges from t = 40 seconds to t = 80 seconds at the same rate. Fig. 7 shows the corresponding simulation results.

The output current of the PV array (b.2) decreases when the solar irradiance (a.1) decreases, however, the voltage (b.1) is

maintained around the same value. This is because the voltage corresponding to the MPP does not change significantly with changing solar irradiance as shown in Fig. 2. Note that the voltage and current corresponding to the MPP at 25 $^0$C and 1000 W/m$^2$ are 401 V and 383.8 A, respectively. The dc link voltage of the PV inverter is not affected by the changing solar irradiance, in fact it is regulated at a constant value to supply the required output voltage.

During the first 60 seconds of Scenario A, since the battery is used for solar smoothing, the power output at the point-of-common-coupling (PCC) is regulated at the chosen 600 kW (f.1) regardless of the changing solar irradiance. From 60 to 80 seconds the battery is charged at 500 kW and from 80 to 100 seconds, the battery is discharged at 500 kW. Note that the frequency at the PCC is fixed at 60 Hz because the microgrid is in grid-connected mode. Small spikes in frequency (e.4 and f.4) are due to minor simulation glitches.

### B. Scenario B: Battery operating in grid-forming mode

Initially (from t = 0 to t = 10 seconds), the microgrid is grid-connected and the PV system injects power into the grid, assuming a constant irradiance. The battery neither charges nor discharges. When the microgrid is suddenly islanded at t = 10 seconds, the battery controller switches to islanded mode to maintain the microgrid's desired voltage and frequency. The load varies between t = 50 and t = 90 seconds while the EV charges from t = 0 to to = 30 seconds and discharge from t = 60 to t = 100 seconds. Fig. 8 shows the results of the simulation for this scenario.

While in grid-connected mode, the voltage at the PCC (f.3) is slightly less than 1 p.u. because the microgrid does not control the voltage at that point. When the microgrid is suddenly islanded at 10 seconds, the voltage regulator in Fig. 4 increases the voltage at the PCC (f.3) to 1 p.u. The active load also slightly increases because the load model is voltage dependent. Since the microgrid is islanded when the power flow at the PCC is not zero, a power spike occurs (d.1, e.1, f1). The battery then manages to maintain the voltage (d.3, f.3) and the frequency (d.4, f.4) at a constant value even when the load varies (between t = 50 and t = 90 seconds) and the solar irradiance decreases (between t = 20 and t = 30 seconds).

### C. Scenario C: Emergency generator operation in islanded mode

In this scenario, the microgrid operates in islanded mode and the emergency generator maintains the desired voltage and frequency. The load varies between t = 50 and t = 90 seconds. The battery charges at 100 kW between t = 10 and t = 100 seconds. The EV charges at 50 kW between t = 0 and t = 100 seconds. Fig 9 shows the simulation results.

The variable load between t = 50 and t = 90 seconds as well as the decision to charge the battery at t = 10 seconds cause frequency oscillations (b.4, d.4, h.4). However, the frequency always stays within ±5 Hz and extending the simulations over a longer duration shows that these oscillations die out. Their amplitude can be reduced by increasing the inertia of the generator, however this causes these oscillations to last longer.
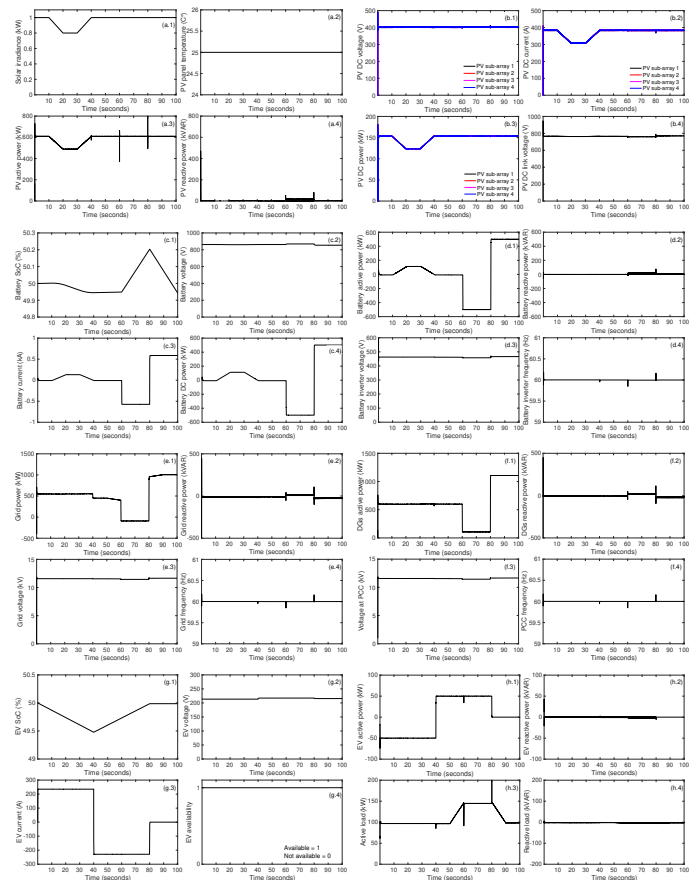


Fig. 7. Simulation results for Scenario A: PV system (a.1-b.4), battery (c.1-d.4), electrical grid (e.1-e.4), PCC (f.1-f.4), EV (g.1-h.2) and load (h.3-h.4).

There are voltage and power spikes (Fig. 9 (d.1, d.3, g.1, g.3)) and a sudden drop in load (Fig. 9 (f.3)) when the battery starts charging at 10 seconds.

### CONCLUSIONS

This paper presented a real-time digital simulation on an OPAL-RT real-time digital simulator of a microgrid being built in by Snohomish PUD in Arlington, WA . This model supports the study of different operating conditions before the microgrid is deployed in the field at the end of 2021.

Once the microgrid is operational, we will compare our simulation results with the actual measured data.

### REFERENCES

[1] M. Farzinfar and M. Jazaeri and N. C. Nair and F. Razavi, "Stability evaluation of microgrid using real-time simulation," in *2014 Australasian Universities Power Engineering Conference (AUPEC)*, Sep. 2014, pp. 1–6.
[2] X. Meng, C. Yang, K. Lin, F. Zhang, J. Wu, and J. Shen, "Research on photovoltaic power system of microgrid based on real-time simulation," in *2017 IEEE Conference on Energy Internet and Energy System Integration (EI2)*, Nov 2017, pp. 1–5.
[3] L. Ghomri, M. Khiat, and S. A. Khiat, "Modeling and real time simulation of microgrids in Algerian Sahara area," in *2018 IEEE International Energy Conference (ENERGYCON)*, June 2018, pp. 1–5.
[4] I. Leonard, T. Baldwin, and M. Sloderbeck, "Accelerating the customer-driven microgrid through real-time digital simulation," in *2009 IEEE Power Energy Society General Meeting*, July 2009, pp. 1–3.
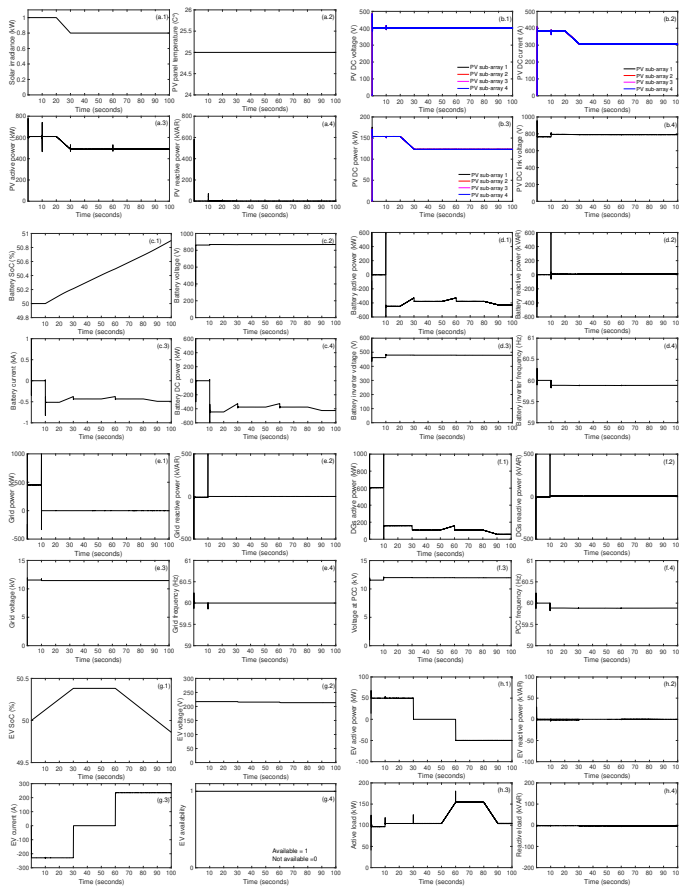
Fig. 8. Simulation results for Scenario B: PV system (a.1-b.4), battery (c.1-d.4), electrical grid (e.1-e.4), PCC (f.1-f.4), EV (g.1-h.2) and load (h.3-h.4).
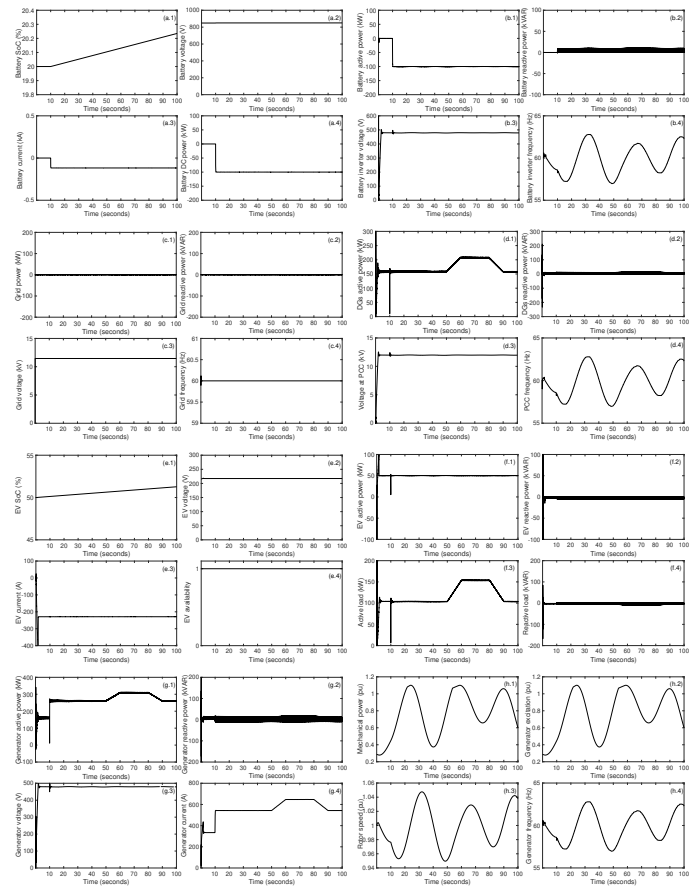


Fig. 9. Simulation results for Scenario C: Battery (a.1-b.4), electrical grid (c.1-c.4), PCC (d.1-d.4), EV(e.1-f.2), load (f.3-f.4) and generator (g.1-h.4).

[5] O. Nzimako and A. Rajapakse, "Real time simulation of a microgrid with multiple distributed energy resources," in *2016 International Conference on Cogeneration, Small Power Plants and District Energy (ICUE)*, Sep. 2016, pp. 1–6.

[6] F. Baccino, A. Brissette, D. Ishchenko, A. Kondabathini, and P. Serra, "Real-time hardware-in-the-loop modeling for microgrid applications," in *2017 6th International Conference on Clean Electrical Power (IC-CEP)*, June 2017, pp. 152–157.

[7] A. Yamane and S. Abourida, "Real-time simulation of distributed energy systems and microgrids," in *2015 International Conference on Sustainable Mobility Applications, Renewables and Technology (SMART)*, Nov 2015, pp. 1–6.

[8] M. Chlela, G. Joos, M. Kassouf, and Y. Brissette, "Real-time testing platform for microgrid controllers against false data injection cybersecurity attacks," in *2016 IEEE Power and Energy Society General Meeting (PESGM)*, July 2016, pp. 1–5.

[9] Snohomish County Public Utility District. Arlington Microgrid Project. [Online]. Available: https://www.snopud.com/?p=3326

[10] C. Keerthisinghe and D. S. Kirschen. (2019) Real-Time Digital Simulation of Microgrid Control Strategies. Renewable Energy Analysis Lab, University of Washington. [Online]. Available: https://labs.ece.uw.edu/real/RTDSmain.html

[11] MathWorks. PV array. [Online]. Available: {https://www.mathworks.com/help/physmod/sps/powersys/ref/pvarray.html}

[12] ——. (250-kW grid-connected PV array). [Online]. Available: https://www.mathworks.com/help/physmod/sps/examples/250-kw-grid-connected-pv-array.html

[13] Mohsin Noman Mustafa, "Design of a grid connected photovoltaic power electronic converter," Master's thesis, Universitet i Tromsø, Jun. 2017.

[14] P. Giroux, G. Sybille, C. Osorio, S. Chandrachood. Average model of a 100-kW grid-connected PV array. MathWorks. [Online]. Available: {https://www.mathworks.com/help/physmod/sps/examples/average-model-of-a-100-kw-grid-connected-pv-array.html}

[15] MathWorks. Simulink battery model. [Online]. Available: {https://www.mathworks.com/help/physmod/sps/powersys/ref/battery.html}

[16] M. Saleh, Y. Esa, Y. Mhandi, W. Brandauer, and A. Mohamed, "Design and implementation of CCNY DC microgrid testbed," in *2016 IEEE Industry Applications Society Annual Meeting*, Oct 2016, pp. 1–7.

[17] MathWorks. Simplified synchronous machine. [Online]. Available: {https://www.mathworks.com/help/physmod/sps/powersys/ref/simplifiedsynchronousmachine.html}

[18] G. Sybille and Tarik Zabaiou. Emergency diesel-generator and asynchronous motor. MathWorks. [Online]. Available: {https://www.mathworks.com/help/physmod/sps/examples/emergency-diesel-generator-and-asynchronous-motor.html}

[19] IDE4L: ideal grid for all. [Online]. Available: https://ide4l.eu

[20] L. Vanfretti, W. Li, A. Egea-Alvarez, and O. Gomis-Bellmunt, "Generic VSC-based DC grid EMT modeling, simulation, and validation on a scaled hardware platform," in *2015 IEEE Power Energy Society General Meeting*, July 2015, pp. 1–5.

[21] L. Vanfretti, N. A. Khan, W. Li, M. R. Hasan, and A. Haider, "Generic VSC and low level switching control models for offline simulation of VSC-HVDC systems," in *2014 Electric Power Quality and Supply Reliability Conference (PQ)*, June 2014, pp. 265–272.

[22] OPAL-RT Techonologies. Microgrid. [Online]. Available: https://www.opal-rt.com/microgrid-overview/